Adenovirus Type-5 Entry and Disassembly Followed in Living Cells by FRET, Fluorescence Anisotropy, and FLIM

Marisa Martin-Fernandez,* Samantha V. Longshaw,* Ian Kirby,† George Santis,† Mark J. Tobin,* David T. Clarke,* and Gareth R. Jones*

*Council for the Central Laboratory of the Research Councils, Daresbury Laboratory, Daresbury, Warrington WA4 4AD, United Kingdom; and †Department of Asthma Allergy and Respiratory Science, King's College London, London SE1 9RT, United Kingdom

ABSTRACT We have used fluorescence resonance energy transfer (FRET) to follow the process of capsid disassembly for adenovirus (Ad) serotype 5 (Ad5) in living CHO-CAR cells. Ad5 were weakly labeled on their capsid proteins with FRET donor and acceptor fluorophores. A progressive decrease in FRET efficiency recorded during Ad5 uptake revealed that the time course of Ad5 capsid disassembly has two sequential protein dissociation rates with half-times of 3 and 60 min. Fluorescence anisotropy measurements of the segmental motions of fluorophores on Ad5 indicate that the first rate is linked to the detachment from the capsid of the protruding, flexible fiber proteins. The second rate was shown to report on the combined dissociation of protein IX, penton base, and hexons, which form the rigid icosahedral capsid shell. Fluorescence lifetime imaging microscopy measurements using a pH-sensitive probe provided information on the pH of the microenvironment of Ad5 particles during intracellular trafficking, and confirmed that the fast fiber dissociation step occurred at the onset of endocytosis. The slower dissociation phase was shown to coincide with the escape of Ad5 from endocytic compartments into the cytosol, and its arrival at the nuclear membrane. These results demonstrate a rapid, quantitative live-cell assay for the investigation of virus-cell interactions and capsid disassembly.

INTRODUCTION

Cell infection by the nonenveloped Ad depends on the orchestrated disassembly program of its large outer protein capsid (Greber et al., 1993). The disassembly of the Ad capsid is required to allow the release of the packaged viral genome, and hence its transportation through the much smaller 30-nm aperture of the nuclear pore complex (Chardonnet and Dales, 1970a; Greber et al., 1997; Trotman et al., 2001; Greber, 2002). The mechanisms governing the outcome of Ad infection have long been the subject of considerable interest, not least because of the apparent advantages of Ad as prospective vectors in gene therapy (Russell, 2000). However, the details of the molecular processes allowing capsid disassembly within the cell are still poorly understood.

The Ad capsid is a complex but well-characterized 80–90-nm icosahedral structure formed from >1200 polypeptides of 11–15 types, within which a 36-kb double strand of DNA is tightly packaged (Burnett et al., 1985). Most abundant are the hexon proteins, which are made up of three copies of hexon polypeptide II, dodecamers of the protein forming the 20 triangular facets of the outer structure. Sixty copies of the penton base polypeptide III are arranged into the 12 vertices of the icosahedron, from which protrude 12 trimeric fiber proteins (Burnett et al., 1985; Van Oostrum and Burnett, 1985; Burnett, 1997). The capsid structure is stabilized by the scaffolding proteins of which VI and IX are the most abundant to the level of 360 and 240 copies, respectively (Burnett, 1997; Greber et al., 1997).

Capsid disassembly occurs during Ad endocytosis and has so far been studied in detail only for one of the 51 human serotypes, Ad serotype 2 (Ad2) during entry in HeLa and A549 cells (Greber et al., 1993; Nakano et al., 2000; Russell, 2000). Ad2 belongs to subgroup C, which also includes the other most extensively studied Ad5 from which replication-deficient vectors capable of transferring genes into non-dividing cells have been derived (Gao et al., 1996; Yeh and Perricaudet, 1997). Ad2 disassembly begins after binding of the virus to its primary cell surface receptor, the coxsackie B virus adenovirus receptor (CAR) via the C-terminal knob domain of the fiber (Chroboczek et al., 1995; Bergelson et al., 1997; Kirby et al., 2000; Nakano et al., 2000). This interaction determines tissue tropism, as CAR binds human adenovirus subgroups A, C, D, and E, infectious for airway epithelial cells, but not subgroup B, whose primary receptor is not known, or one of the two fibers types of subgroup F, which targets differentiated enterocytes (Defer et al., 1990; Stevenson et al., 1995; Russell, 2000). After cell adsorption, the first disassembly event is the dissociation of fibers, which is thought to be mediated by the interaction between the RGD motif of the penton base in the Ad2 capsid and its αv-β3/β5 vitronectin-binding integrin cell surface receptors (Wickham et al., 1993; Stewart et al., 1997). This interaction is also known to regulate Ad-mediated cell signaling, viral endocytosis, and endosomal transport (Greber, 2002; Rauma et al., 1999; Wang et al., 1998; Li et al., 1998; Wickham et al., 1994). After the loss of the fibers, the second disassembly event is the dissociation of the penton base

Submitted October 1, 2003, and accepted for publication May 11, 2004.

Address reprint requests to Gareth R. Jones, E-mail: g.r.jones@dl.ac.uk.

0006-3495/04/08/1316/12 $2.00

doi: 10.1529/biophysj.103.035444

(Greber et al., 1993). This event is also mediated by penton interactions with integrins and occurs ~15 min after Ad2 internalization, coinciding with the escape of the virus from endocytic vesicles into the cytosol (Blumenthal et al., 1986; Pastan et al., 1986; Greber et al., 1993; Seth, 1994). The escape into the cytosol depends on Ad2 virions having efficiently shed its fibers at the cell surface (Nakano et al., 2000). Having passed into the cytosol, the partially disassembled genome-containing Ad2 particles make use of microtubules and microtubule-dependent motors to be transported toward the cell nucleus (Leopold et al., 2000; Suomalainen et al., 1999). Simultaneously, protein IX, a cementing factor that binds the hexons together, is removed from Ad2 over a period between 30 and 60 min after entry (Greber et al., 1993). The time of arrival at the nucleus is correlated with the last step of capsid disassembly, the loss of the hexon component, which occurs at the nuclear membrane after the docking of Ad2 at nuclear pore complexes (Greber et al., 1997, 1993).

In other Ad serotypes capsid disassembly is less well characterized. It is known, however, that the above pattern of disassembly is not universal. For example, the non-CAR binding subgroup B Ad serotype 3 (Ad3) and Ad serotype 7 (Ad7) do not appear to loose the fibers at the cell surface, and are retained in late endosomal and lysosomal compartments with consequentially lower infection rates (Chardonnet and Dales, 1970b; Miyazawa et al., 1999, 2001; Russell, 2000). It would be useful therefore to gain an understanding of the life cycles of different Ad serotypes and chimeric viruses as part of a strategic approach of Ad targeting to different cell tissues for therapeutic purposes (Russell, 2000). However, acquiring this amount of time-course data using conventional cell-free methods is a challenging and lengthy task, which requires immunochemistry and gel electrophoresis measurements on a different cell lysate per datum (Greber et al., 1993). This probably accounts for the limited amount of time-based information available on capsid disassembly. Measurements in living cells using the noninvasive technique of fluorescence microscopy, go a long way to providing the cellular distribution of viral material in real time (Leopold et al., 2000, 1998; Nakano and Greber, 2000), but cannot report on capsid disassembly events because they do not have the spatial resolution.

Here we have used fluorescence resonance energy transfer (FRET) and fluorescence anisotropy for the real-time measurement of the time course of capsid disassembly of subgroup C Ad5 during uptake in living cells. FRET is a process by which excited-state energy of a fluorescent molecule (donor) after photon absorption is transferred to a suitable neighboring molecule (acceptor). This process competes with and therefore quenches the donor fluorescence by shortening its fluorescence lifetime. FRET occurs whenever donor and acceptor molecules are separated by a distance $<\sim 10$ nm, the efficiency of which is dependent on the inverse sixth power of donor to acceptor distance and on the relative orientation of the donor and acceptor transition dipoles (Lakowicz, 1983). Our experimental strategy has been to bind both donor and acceptor dye moieties randomly to the capsid proteins of the intact virus and use the anticipated decrease in FRET efficiency as measured by the increase in the fluorescence lifetime of the donor to monitor capsid disassembly in real time. The time course of the fluorescence anisotropy decay of donor-labeled Ad5 was recorded in conjunction with the FRET measurements to investigate the dependence of the FRET results on the relative orientation between donors and acceptors (Lakowicz, 1983). The anisotropy decay is proportional to the difference between the fluorescence decay profiles in the directions parallel and perpendicular to the polarized excitation light (Lakowicz, 1983). Due to photoselection the fluorophore emission is polarized along the direction of the polarization of the excitation light. Rotational motions of fluorophores can depolarize the fluorescence emission, resulting in more photons emitted in the perpendicular direction. Anisotropy decay data can therefore reveal the diffusive motions of the fluorophores on Ad5 and the restrictions to their angular displacement imposed by their binding to the proteins in the capsid. Fluorescence lifetime imaging microscopy (FLIM) and confocal laser scanning microscopy (CLSM) were also used to evaluate the pH of the immediate environment of Ad5 and its rate of uptake via the measurement of the fluorescence lifetime of an Ad5-bound pH probe. Fluorescence lifetime measurements are more challenging than measurements based on fluorescence steady-state intensities, but have the advantage of providing quantitative results largely free from artifacts such as photobleaching and radiative transfer (Day and Piston, 1999; Martin-Fernandez et al., 1996). In these experiments we have demonstrated two distinct phases of Ad5 capsid disassembly that can be attributed to the dissociation of fibers, and to the combined dissociation of penton, hexon, and protein IX. The methodology presented could form the basis for other systematic studies of the mechanisms of entry and disassembly of different Ad serotypes in various cell types.

MATERIALS AND METHODS

Mammalian tissue culture

A549 cells (Caucasian lung carcinoma) purchased from the European Collection of Animal Cell Cultures (Porton Down, UK) were cultured in Dulbecco's modified eagle medium (DMEM) supplemented with 10% (v/v) fetal calf serum (FCS), 1% (v/v) 200 mM glutamine (final concentration 2 mM), and 0.4% (v/v) gentamycin (final concentration 50 μg/ml) (Life Technologies, Paisley, UK). CHO-CAR cells (a kind gift from Dr. G. E. Blair, Leeds University, Leeds, UK) were cultured in minimal essential medium (MEM)-α medium augmented with the same supplements as above. Cells were then incubated at 37°C in the presence of 5% CO_2 until an ~70% confluent monolayer had formed (~2–3 days).

Virus culture

Ad5 was obtained from the Centre of Applied Microbiology and Research (Porton Down, UK). A549 cells were infected with Ad5 at a multiplicity of

infection (m.o.i.) of 0.1 plaque-forming units (p.f.u.) per cell. Incubation with virus was continued for 5 days or until a 100% cytopathic effect was observed. Infected cells were pelleted by centrifugation at 1500 rpm for 10 min at 4°C, resuspended in 10 ml phosphate buffered saline (PBS) and broken open by three rounds of freeze thawing (−80°C). Viruses were extracted from the cell debris by addition of 1,1,2 trichloro-trifluoroethane followed by centrifugation at 2000 rpm for 15 min at 4°C. The top, aqueous layer contained the virus. Cesium chloride was then added to the order of 0.51 times this volume. Aliquots (10 ml) were centrifuged at 36,000 rpm for 18 h at 4°C. The translucent white band of virus was harvested and recentrifuged on a discontinuous cesium chloride gradient, containing 3 ml of 1.33 g/cm^3 CsCl and 2 ml of 1.45g/ cm^3 CsCl and the virus band once again collected. The concentration of virus was measured by its absorbance at 260 nm.

Virus titration

A 10-fold dilution series of virus was prepared using DMEM. To each well of a 24 well plate, 0.5 ml of A549 cells at a concentration of 3 × 105 cells/ml was added. Each dilution (100 μl) of the stock virus (usually 1 part in either 10^6, 10^7, or 10^8) were each added to six wells of the 24-well plate. The remaining six wells contained no virus to act as negative control. The plate was then incubated at 37°C and 5% CO_2 overnight. After this period, 1 ml of 2× DMEM (containing 3% carboxymethyl cellulose) was added to each well. After a further 6 days of incubation at 37°C and 5% CO_2, the wells were fixed by adding 1 ml of 10% formaldehyde in PBS for 20 min. The wells were then washed with water and stained with 1 ml of 0.1% methyl violet for 20 min, before being washed again with water and then left to air dry. The plaques were counted and the virus titre calculated.

Fluorescence labeling

Solvent-exposed amino groups of Ad5 capsid proteins were labeled with Alexa 488, Alexa 594, and fluorescein (Molecular Probes, Leiden, The Netherlands). Alexa 488, Alexa 594, and fluorescein isothiocyanate (FITC) were dissolved in 100 μl of water (FITC in DMSO) and then 1 M sodium bicarbonate (final concentration 50 mM) was added to obtain pH 8.0. Dye aliquots of 100 μl containing either 6.5 μg, 7.8 μg, or 4 μg of the dyes above, respectively, were added to purified virus and left for 45 min on a shaker platform. Hydroxylamine (final concentration 50 mM) was then added to bind unattached dye before gel filtration to separate unbound dye (Sephadex G-50 beads, Sigma, St. Louis, MO). Elution of labeled virus was monitored by absorbance at 280 nm. Conjugates were assayed in a spectrometer by using molar extinction coefficients at 260 nm, 488 nm, 490 nm, and 594 nm. Small aliquots of the virus/dye conjugates were stored at −80°C in the dark in PBS containing 10% (w/v) glycerol. To determine which capsid proteins incorporate dye molecules, labeled Ad5 was boiled in sodium dodecyl sulfate polyacrylamide gel electrophoresis (SDS-PAGE) sample buffer. The virus samples were subjected to acrylamide gradient (4–12%) gel electrophoresis using Laemmli buffers (Laemmli, 1970). Densitometric analysis of Alexa 488 and fluorescein-labeled Ad5 was carried out using a Molecular Dynamics-Storm 860 (Buckingham, UK) fluorescence imager.

Sample preparation

Coverslips were placed into each well of a six-well dish and seeded with 3 ml of cells at a concentration of 3 × 105 cells/ml. The following day, the media was changed to media containing 1% serum. Coverslips were incubated overnight and the medium in the wells replaced with serum-free media three hours before required. Coverslips were washed four times with ice-cold PBS, and transferred to a sample dish on ice. Then 100 μl of a 10^8 labeled virus/ml ice-cold solution (in PBS, no glycerol) was added to the cells for 1 h in the dark at 4°C. The coverslips were washed four times with ice-cold PBS to remove any unbound virus and then loaded into a temperature-controlled sample stage. The temperature of the samples was measured using a thermocouple located within the cell holder and recorded in real time during the experiments.

Fluorescence measurements

Fluorescence decays were recorded using a lifetime microfluorimeter at the synchrotron radiation source (SRS) (Daresbury Laboratory, Warrington, UK) using horizontally polarized pulsed synchrotron radiation as excitation light and an emission polarizer at the magic angle (54.7°) in the emission path as previously described (Martin-Fernandez et al., 1996). Fluorescence anisotropy decays were collected by measuring the components of the fluorescence decay parallel [$I_{par}(t)$] and perpendicular [$I_{per}(t)$] to the linearly polarized excitation light: $r(t) = (I_{par} - I_{per}) / (I_{par} + 2I_{per})$ with a polarizing microscope as described elsewhere (Martin-Fernandez et al., 1998). Confocal reflection and fluorescence images were collected using a purpose-built confocal microscope equipped with a continuous wave Ar+ laser as a light source (Van der Oord et al., 1996). Pinholes (50 μm) were used in the excitation and emission paths. FLIM data were collected with the confocal microscope using a pulsed, frequency-doubled Ti:Sapphire laser as light source, which delivered 480 nm wavelength light pulses of 100 fs with a repetition rate of 76 MHz (Coherent, Santa Clara, CA). Laser light was delivered to the sample via a dichroic mirror (51004v2, Chroma Technology, Rockingham, VT) and a 1.3 n.a. oil immersion objective (Carl Zeiss, Oberkochen, Germany). The fluorescence emission was collected using a band-pass emission filter (HQ535/50m, Chroma Technology, Rockingham, VT). Confocal images were 512 × 512 pixels in size collected using a photomultiplier tube (R3896, Hamamatsu, Bridgewater, NJ). FLIM images were collected using a time-correlated single-photon counting FLIM module (SPC-730) (Becker & Hickl, Berlin, Germany) and a photomultiplier tube (PMH-100-1, Hamamatsu). The FLIM images were 256 × 256 pixels in size and the image acquisition time was 2 min.

Data analysis

FLIM data were analyzed using SPCImage 2.5 (Becker & Hickl, Berlin, Germany). Briefly, the fluorescence decay data in each pixel were reconvoluted with the excitation profile and best fitted by least-squares analysis to the biexponential law, which returned flat residuals (data minus fit), and a goodness of fit χ^2 between 0.8 and 1.2. The mean fluorescence lifetime was calculated using $\langle\tau\rangle = (\alpha_1\tau_1 + \alpha_2\tau_2) / (\alpha_1 + \alpha_2)$, where α_i are the preexponential terms and τ_i the fluorescence lifetime components returned by the fit. Fluorescence decays recorded in the lifetime microfluorimeter (pH calibration) were analyzed as described above with the program FLUOR. For FRET measurement in cells fluorescence decays were fitted using FLUOR after subtraction of the fluorescence background. The ratio of signal to background is set by the program according to frame acquisition time (as described in Martin-Fernandez et al., 2002). The background contains an approximate 60:40 ratio of the background of the microscope and autofluorescence. The variation experimentally recorded for the background is ±10% (see Fig. 7 *B*). Fits were performed for ratios signal/background varying up to ±10% in steps of 2% above and below the default value set by the program. The ratio that returned the best fits with clear χ^2 minima was chosen. In the majority of cases the default value set by the program returned the best analysis.

RESULTS

Intracellular accumulation of Ad5 followed by CLSM and FLIM

The time course of Ad5 uptake was investigated in two cell lines, A549 and CHO-CAR. Cells were infected with Ad5

conjugated with fluorescein (Fluor-Ad5) or Alexa 488 (Al_{488}-Ad5). The degree of dye labeling of the virus was guided by a plot of virus efficacy measured by the titre of plaque-forming units versus the amount of dye used in the labeling reaction (Fig. 1). A compromise between strong fluorescence signals and high viral titre was achieved by ensuring titres in excess of 80% of those observed for unlabeled virus throughout this work. The amounts of reactive dye employed (<10 μg/ml) also ensured conjugations of less than one dye molecule per capsid protein.

Fig. 2 *A* shows a confocal reflection image of A549 cells infected with Al_{488}-Ad5 at 4°C. By cooling the cells, Ad5 cell attachment was experimentally separated from virus endocytosis, which only occurs efficiently at temperatures of ~37°C (Hong et al., 1997). The fluorescence confocal image acquired from the same field of view and under the same conditions as Fig. 2 *A*, shows Al_{488}-Ad5 particles localized at the plasma membrane, where individual viruses are clearly detectable (Fig. 2 *B*). One hour after the temperature of the cells had been raised to 37°C most viruses appear to be inside the cells and localized around the cell nuclei (Fig. 2 *D*). The piezoelectric scanning of the *z* axis of the microscope allows us to determine that the images were recorded at a height plane *z* intersecting the cell nuclei. These data show that fluorescent Ad5 conjugates follow a similar entry pathway to that previously observed for the uptake in HeLa and A549 cells of Ad2 and Ad5 (Leopold et al., 1998; Miyazawa et al., 2001; Nakano and Greber, 2000).

The pathway of internalization of Ad5 was also followed in CHO-CAR cells using CLSM and FLIM. CHO-CAR cells are CHO cells that have been transfected with the CAR cDNA and permanently express CAR, the Ad5 cell attachment receptor, on their cell surface and as a result have been rendered permissive for Ad5 infection (Bergelson et al., 1997). The CHO-CAR cell line expresses ~80,000 CAR receptors per cell, i.e., ~10-fold more than the A549 cell line (Bergelson et al., 1997; McDonald et al., 1999). For

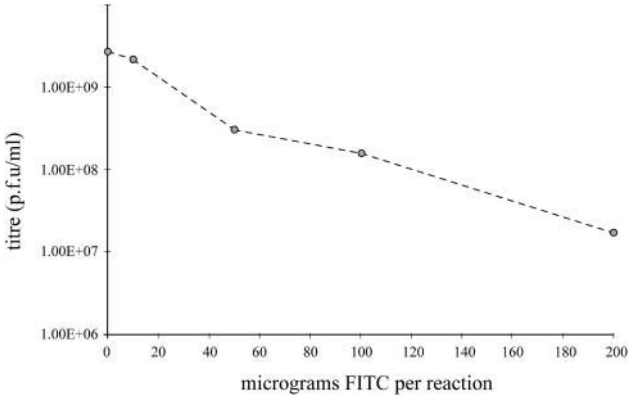

FIGURE 1 Titration results from Ad5 labeled with increasing amounts of fluorescein as described in the methods showing the decrease in the viability of virus fluorescent conjugates as the ratio dye/virus was increased.

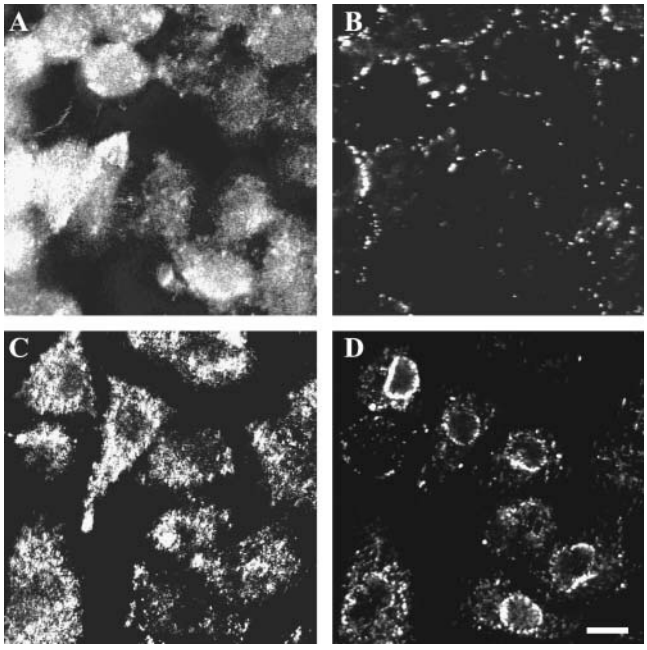

FIGURE 2 (*A*) Reflection confocal image of A549 cells infected with Al_{488}-Ad5 and held at 4°C. (*B*) Fluorescence confocal image recorded from the same field of view showing the distribution of Al_{488}-Ad5 at 4°C. (*C*) Reflection confocal image of A549 cells infected with Al_{488}-Ad5 after being kept for 1 h at 37°C. (*D*) Fluorescence confocal image recorded from the same field of view showing the corresponding distribution of Al_{488}-Ad5 at 37°C. The thickness of the sections is 0.7 μm. Bar = 10 μm.

these measurements Ad5 was conjugated to the optically pH-sensitive dye fluorescein (Fluor-Ad5) so as to detect the lower pH of endosomal compartments via FLIM measurement of pH-dependent fluorescence lifetime changes (see below). Fluorescence images of Fluor-Ad5 in CHO-CAR cells infected and held at 4°C show viruses decorating the plasma membrane of these cells in a similar fashion as previously found for A549 cells (Fig. 3 *A*). Fluorescence images recorded 7 min after the onset of a temperature jump from 4°C to 37°C show initial stages of Fluor-Ad5 uptake (Fig. 3 *B*). The temperature in the cells takes ~4 min to reach 37°C, hence the image in Fig. 3 *B* reports on the extent of viral internalization 3 min after the temperature in the cells reached the physiological value. An hour after the temperature had been raised to 37°C most of the fluorescence signal was again localized around the cell nuclei (Fig. 3 *C*) resulting in less fluorescence at the plasma membrane and the appearance of gaps between adjacent cells. These data show a time course of Ad5 delivery to the nucleus similar to that which we observed for A549 cells. Images of CHO-CAR cells exposed to unlabeled virus (native Ad5) taken under the same illumination conditions as in Fig. 3, *A–C*, show the level of cell autofluorescence (Fig. 3 *D*). We found the ratio between virus signal and cell autofluorescence to be significantly larger for CHO-CAR than for A549 cells (data not shown). In CHO-CAR cells infected with Fluor-Ad5, autofluorescence accounts for ~1/10th of the total intensity.

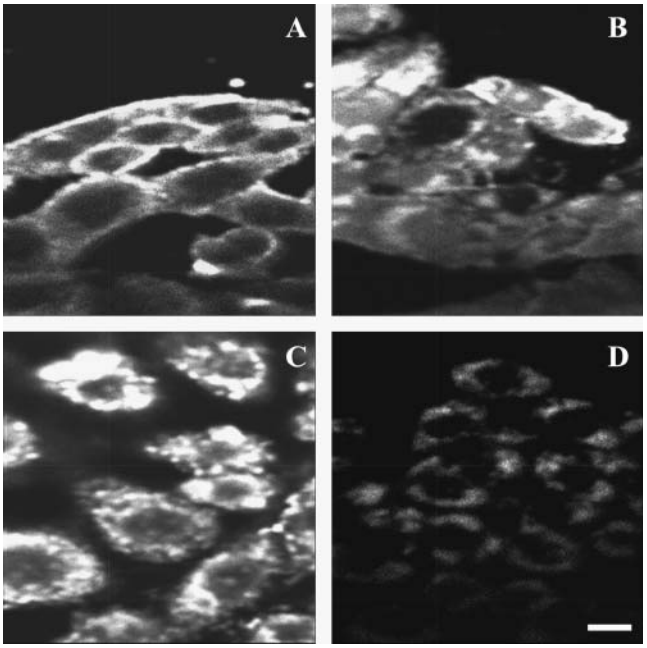

FIGURE 3 (*A*) Fluorescence confocal image of CHO-CAR cells infected with Fluor-Ad5 and held at 4°C. (*B*) Image from a different field of view recorded 3 min after the temperature in the cells reached 37°C. (*C*) Image collected 1 h after the temperature was raised to 37°C. (*D*) Fluorescence confocal image of CHO-CAR cells infected with native Ad5 taken under the same illumination and detection conditions. The thickness of the sections is 0.7 μm. Bar = 10 μm.

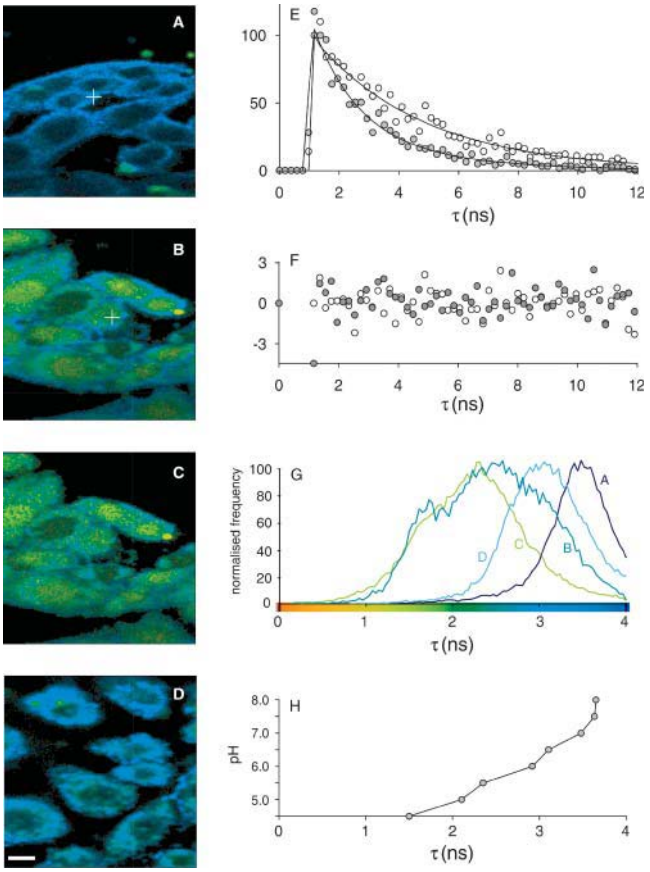

FIGURE 4 (*A*) Example of fluorescence lifetime image showing the cellular distribution of the first order average fluorescence lifetime in CHO-CAR cells infected with Fluor-Ad5 and held at 4°C, color coded according to the bar in the *x* axis of Fig. 4 *F*. (*B*) As in panel *A* in a different area of the same sample 3 min after the temperature of the cells reached 37°C. (*C*) Same area as panel *B* 7 min later. (*D*) As in panel *A* 60 min after the temperature of the cells reached 37°C. The thickness of the sections is 0.7 μm. Bar = 10 μm. (*E*) Example of fluorescence decays measured for the pixels marked by a cross in panels *A* and *B*, and analyzed to the biexponential law (0.194 ns per channel). (*F*) Residuals of this analysis. (*G*) Normalized distributions of the mean fluorescence lifetime of Fluor-Ad5 (τ) across the FLIM images *A–D* as indicated. (*H*) Mean fluorescence lifetime values of Fluor-Ad5 in Tris citrate buffer solution at pH values of 4.5–8.

The increase in contrast is consistent with the expected higher level of Ad5 binding to CAR in CHO-CAR cells, and facilitated the accurate subtraction of the autofluorescence from fluorescence decay data in the FRET experiments below. Specific binding of Ad5 to CAR was confirmed by the absence of signal above autofluorescence in CHO cells, which do not express CAR (data not shown).

To further investigate the pathway of Ad5 cell entry, FLIM was used to measure the pH of the microenvironment of virions internalized at early stages of the infection process. Fluorescence decay data from Fluor-Ad5 were stored in time channels for each pixel of confocal images in Fig. 3. Typical fluorescence decays corresponding to the pixels marked in Fig. 4, *A* and *B*, are shown in Fig. 4 *E*. The fluorescence decays were fitted for each pixel as described in Materials and Methods. The residuals (data minus fit) of this analysis are shown in Fig. 4 *F*. The resulting fluorescence lifetime maps (Fig. 4, *A–D*) show images of the mean fluorescence lifetime (τ) obtained by assigning a color to each pixel according to its fluorescence lifetime using the scale given in the *x* axis of Fig. 4 *G*. The temporal histograms of the distribution of the mean fluorescence lifetime of Fluor-Ad5 across the image pixels are shown in Fig. 4 *G*. The positions and widths of the fluorescence lifetime distributions of Fig. 4 *G* account for the color assignment in Fig. 4, *A–D*. The FLIM results are summarized in Table 1. To investigate the contribution from cell autofluorescence FLIM data were collected under the same illumination conditions from CHO-CAR cells infected with native-Ad5 (Fig. 5). These maps show the distribution of the fluorescence lifetime of cell autofluorescence to be significantly different to the distributions from cells infected with Fluor-Ad5 (Fig. 4, *A–D*). We also found that the fluorescence lifetime distribution of cell autofluorescence does not vary with time for the duration of the experiment.

The changes in the fluorescence lifetime of Fluor-Ad5 with pH were calibrated in a control set of different pH Tris-citrate buffer solutions by recording the fluorescence decays of Fluor-Ad5 at pH values from 4.5 to 8. These data show changes in the fluorescence lifetime of Fluor-Ad5 from a value of 3.64 ns at pH 8 to 1.50 at pH 4.5, showing that Fluor-Ad5 can be used as an indicator of intracellular pH

TABLE 1 Fluorescence lifetime distribution parameters from FLIM and their correlated pH values

Time after internalization	Distribution maximum (τ_{max})	pH max	Distribution range (FWHM)*	pH range (FWHM)
Cells at 4°C	3.48 ns	7.0	3.11 ns $\leq \tau \leq$ 3.86 ns	6.6 $\leq$ pH $\leq$ 8.0
3 min at 37°C	2.51 ns	5.8	1.54 ns $\leq \tau \leq$ 3.43 ns	4.5 $\leq$ pH $\leq$ 7.0
10 min at 37°C	2.34 ns	5.5	1.66 ns $\leq \tau \leq$ 2.91 ns	4.6 $\leq$ pH $\leq$ 6.0
60 min at 37°C	3.10 ns	6.5	2.50 ns $\leq \tau \leq$ 3.56 ns	5.7 $\leq$ pH $\leq$ 7.2

*Fluorescence lifetime values within the FWHM of the distributions in Fig. 4 *F*.

(Fig. 4 *H*). The fluorescence lifetime distribution from a monodisperse fluorescein sample in a dilute solution at pH 7 was measured to be Gaussian and centered at $\tau = 4.00$ with a full-width half maximum (FWHM) of ± 0.28 ns (data not shown). The larger widths of the fluorescence lifetime distributions in Fig. 4 *G* must therefore be due to viruses being simultaneously localized in microenvironments at different pH values.

The correlation between fluorescence lifetime and pH shown in Fig. 4 *H* was used to map the FLIM results to the pH of Ad5 microenvironment (Table 1). The fluorescence lifetime distribution maximum ($\tau = 3.5$ ns) from Fluor-Ad5 particles in cells held at 4°C (Fig. 4 *G*) reports on the viruses being in an environment at a mean pH value of 7. This result is consistent with the localization of Fluor-Ad5 at the plasma membrane and exposed to the neutral extracellular milieu (Fig. 4 *A*). After 3 min at 37°C the shift of the fluorescence lifetime distribution toward shorter values (Fig. 4 *G*) shows a substantial proportion of internalized Ad5 particles exposed to an acidic environment (Fig. 4 *B*). A small number of viruses, however, still remained at the plasma membrane at neutral pH (*blue* features in Fig. 4 *B*). Seven minutes later (Fig. 4 *C*) most blue features have disappeared, which suggests that after 10 min at 37°C most viruses were located within acidic vesicles. This is reflected by a further shift of the fluorescence lifetime distribution toward shorter values. The differences at 3 and 10 min (Fig. 4, *B* and *C*) were not immediately apparent from the confocal images alone (Fig. 3, *B* and *C*) demonstrating the advantage of the FLIM measurement. After an hour's internalization the fluorescence lifetime distribution shifts back toward longer fluorescence lifetimes (Fig. 4, *D* and *G*). The maximum of the fluorescence lifetime distribution from Fig. 4 *D* is $\tau \sim 3.1$ ns, which corresponds to pH $\sim$ 6.5 (Fig. 4 *H*). As the pH of endosomes is below 6.5 (Miyazawa et al., 2001) the data show that only about half of the viruses remain within acidic vesicles an hour after the onset of internalization. In agreement with previous work (Miyazawa et al., 2001), the longer fluorescence lifetimes in the fluorescence lifetime distribution of Fig. 4 *D* report on internalized viruses that have escaped from the endocytic pathway to the pH neutral cytosol and are located in the vicinity of the nuclear envelope.

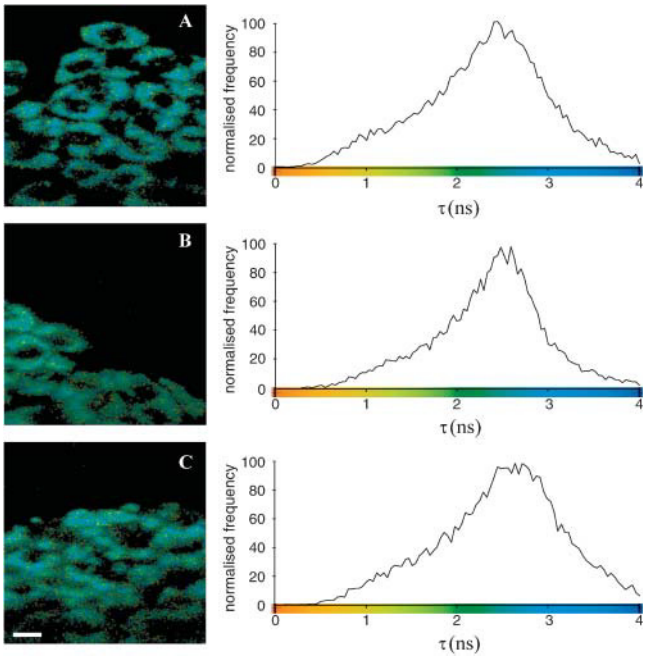

FIGURE 5 (*A*) Left column is an example of fluorescence lifetime image showing the cellular distribution of the first order average fluorescence lifetime in CHO-CAR cells infected with native Ad5 color coded according to the bar in the *x* axis on the right-hand column, recorded after raising the temperature to 37°C. (*B*) As in panel *A* in a different area, recorded 10 min later. (*C*) After an additional 10 min. The right-hand column shows the normalized distributions of the mean fluorescence lifetime across the FLIM images.

Monitoring Ad5 disassembly by real-time FRET and fluorescence anisotropy

Capsid disassembly was investigated by fluorescence lifetime-based FRET measurements performed on Ad5 simultaneously conjugated with Alexa 488 (donor) and Alexa 594 (acceptor) at a donor/acceptor ratio of ~1:1. Densitometry analysis of SDS-PAGE gels using ImageQuant version 5.0 software (Molecular Dynamics) indicated that ~73% of the Alexa fluorophore was incorporated into hexon, 6% was found in penton base, ~9% in fiber/IIIa, and ~12% in protein IX (data not shown). These results are in broad agreement with a previous report (Greber et al., 1997). Western analysis using the fiber-specific antibody 4D2 (Abcam, Cambridge, UK) was also used to confirm the presence of labeled fiber. The total degree of labeling employed was calculated to be ~1000 dyes per capsid (Fig. 6 *A*). Taking into consideration that fibers, pentons, hexons, and protein IX are accessible to lysine-binding dyes this degree of labeling is equivalent to less than one dye

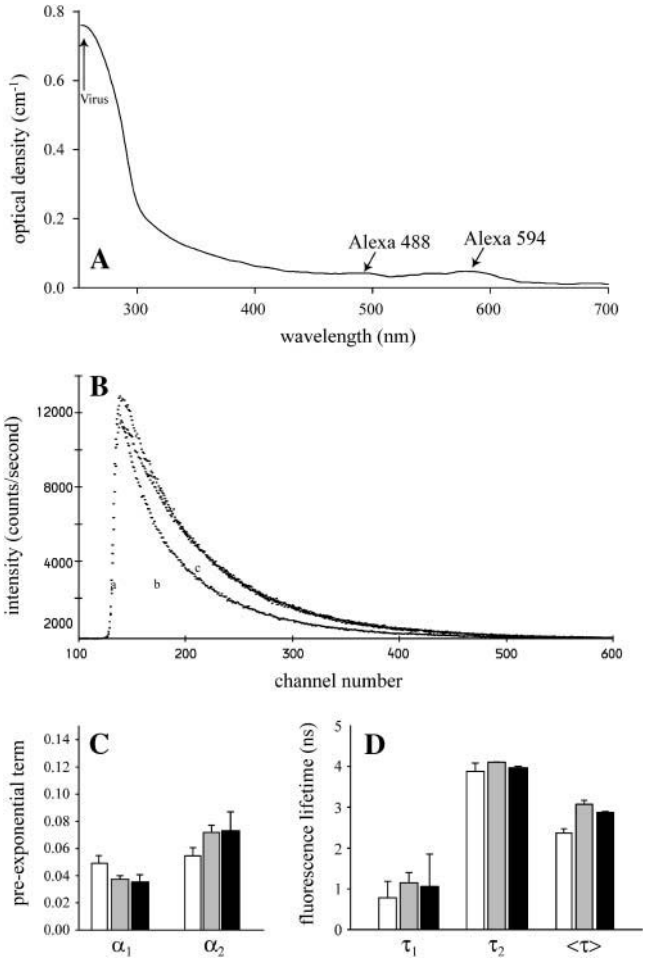

FIGURE 6 (*A*) Absorption spectrum of $Al_{488+594}$-Ad5, showing a labeling ratio of <1000 dyes of each type per virus capsid, calculated from published extinction coefficients (Leopold et al., 1998). (*B*) Fluorescence decays of a PBS solution + 10% (w/v) glycerol at 4°C containing intact 3 × 1011 $Al_{488+594}$-Ad5 particles per ml (*a*), intact Al_{488}-Ad5 particles (*b*), and broken $Al_{488+594}$-Ad5 after treatment with 1% SDS and heat (*c*). The fluorescence decays were collected over 700 channels at 0.0472 ns per channel. (*C*) Histogram of the variation of preexponential terms on three different samples of intact $Al_{488+594}$-Ad5 particles (*open bars*), intact Al_{488}-Ad5 particles (*shaded bars*), and broken $Al_{488+594}$-Ad5 (*solid bars*). (*D*) Corresponding histogram of the variation of the fluorescence lifetime components and average fluorescence lifetime for intact $Al_{488+594}$-Ad5 particles (*open bars*), intact Al_{488}-Ad5 particles (*shaded bars*), and broken $Al_{488+594}$-Ad5 (*solid bars*).

molecule per accessible capsid protein (Van Oostrum and Burnett, 1985). The combination of Alexa 488 and Alexa 594 as donor/acceptor pair is well suited to measure FRET within large particles, such as Ad5. The Förster radius (R_o) for this FRET pair, which is the distance at which the efficiency of FRET is 50%, has been calculated from spectroscopy data from dye molecules in solution to be R_o = 6 nm (Haugland, 2002, and M. L. Martin-Fernandez, unpublished results). This value is large enough to allow this FRET pair to report on donor-acceptor distances as large as 9 nm (Martin-Fernandez et al., 2002), or a tenth of the diameter of the Ad particle.

Before FRET measurement in cells we investigated whether FRET could be detected in intact Ad5 in physiological buffer solution at 4°C when the viruses are simultaneously labeled with donor and acceptor dye ($Al_{488+594}$-Ad5). The fluorescence decay of the donor moiety in $Al_{488+594}$-Ad5 particles was recorded to investigate the presence of FRET-derived quenching (Fig. 6 *A*) and the data were best fitted by the biexponential law (see Materials and Methods). This analysis returned a mean fluorescence lifetime of 2.4 ns. Donor fluorescence decay data were also recorded from donor-only labeled Ad5 (Al_{488}-Ad5) in buffer solution. Donor-labeled viruses were conjugated using the same amount of Alexa 488 as that used in $Al_{488+594}$-Ad5 conjugations, but in this case no acceptor was added. The analysis of the fluorescence decay data for Al_{488}-Ad5 returned a fluorescence lifetime of 2.9 ns, which is 0.5 ns longer than the value measured for $Al_{488+594}$-Ad5, suggesting the presence of FRET in $Al_{488+594}$-Ad5. To confirm that the fluorescence lifetime quenching of the donor in $Al_{488+594}$-Ad5 was due to FRET, $Al_{488+594}$-Ad5 particles were disassembled by the addition of 1% SDS at 60°C for 30 min. After this procedure, the fluorescence lifetime of the donor was measured to be 3.1 ns. This is slightly longer than the value measured for Al_{488}-Ad5 in buffer solution and may represent the change in environment of the dye due to action of the detergent. From these results, the efficiency of FRET (E) in intact $Al_{488+594}$-Ad5 was calculated to be 0.17 using $E = 1 - \tau_{da}/\tau_a$, where τ_{da} and τ_d are the fluorescence lifetimes in the presence and absence of acceptor (Lakowicz, 1983).

To measure the time course of the efficiency of FRET during $Al_{488+594}$-Ad5 entry in CHO-CAR cells, fluorescence decay profiles of the donor fluorophore were recorded in consecutive time frames using a lifetime microfluorimeter under wide-field illumination conditions (Martin-Fernandez et al., 1996). Photobleaching in the confocal FLIM measurements prevented the continuous collection from the same area of the sample of images and time-course data for the duration of the experiment, which was two hours. Therefore, for FRET time-course measurement the spatial resolution of the microscope was sacrificed to allow continuous measurement on the same area at the required time resolution (Martin-Fernandez et al., 1996). Fluorescence decay data were recorded in time frames from cells infected with $Al_{488+594}$-Ad5, Al_{488}-Ad5, and native Ad5. The decays recorded from cells infected with native Ad5 were used to quantify the level of the fluorescence background arising from all components other than fluorescently labeled viruses. Fig. 7, *A* and *B*, show that the background accounted for ~30% of the total fluorescence measured in CHO-CAR cells infected with $Al_{488+594}$-Ad5. The background is partly due to wide-field microscope optics (~60%) and partly due to CHO-CAR cell autofluorescence (~40%) showing that autofluorescence accounts for ~1/8th of the signal from cells infected with $Al_{488+594}$-Ad5. The fluorescence decay of the background was best fitted by a three-exponential decay

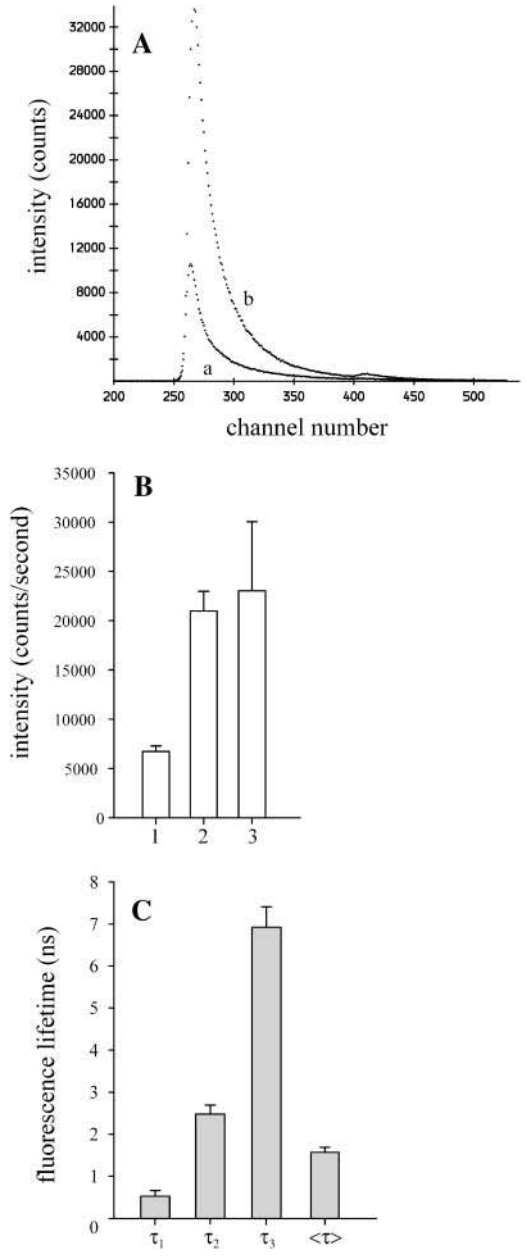

FIGURE 7 (*A*) Fluorescence decay of CHO-CAR cells infected with native Ad5 (*a*) and $Al_{488+594}$-Ad5 (*b*) at 4°C recorded in identical time frames. (*B*) Histogram of the fluorescence intensity from cells infected with native Ad5 (*1*), $Al_{488+594}$-Ad5 (*2*), and Al_{488}-Ad5 (*3*). (*C*) Histogram of the variation of the fluorescence lifetime components and average fluorescence lifetime returned by the analysis of fluorescence decays from CHO-CAR cells infected with native Ad5 (background fluorescence) and maintained at 4°C to inhibit endocytosis. The fluorescence decays were collected over 500 channels at 0.0914 ns per channel.

(Fig. 7 *C*). The shortest lifetime component was mostly due to instrument background whereas the two longer lifetime components arose mainly from cell autofluorescence (Martin-Fernandez et al., 1996). The resulting average fluorescence background lifetime in cells held at 4°C was 1.6 ns (Fig. 7 *C*). This lifetime value is predictably shorter than that previously observed by FLIM (Fig. 5) because the contribution from the instrument background from wide-field optics was not present in the confocal microscopy images.

The fluorescence decays from cells infected with Al_{488}-Ad5 and $Al_{488+594}$-Ad5 were background subtracted using the fluorescence/background decay ratio that returned the best goodness of fit (χ^2) and best fitted by the biexponential law (see Materials and Methods). This analysis returned donor fluorescence lifetime values of 2.8 ± 0.1 ns for Al_{488}-Ad5 and 2.3 ± 0.09 ns for $Al_{488+594}$-Ad5 in cells held at 4°C, which corresponds to an efficiency of transfer for $Al_{488+594}$-Ad5 bound to CAR at the plasma membrane of $E = 0.18$ (Fig. 8, *B–D*). This value compares well with that previously found in buffer solution. After endocytosis was triggered by a temperature jump from 4°C to 37°C the average fluorescence lifetime of CHO-CAR cells infected with native Ad5 showed the time dependence illustrated in Fig. 8 *A*. The initial decrease in fluorescence lifetime measured for both Al_{488}-Ad5 and $Al_{488+549}$-Ad5 (Fig. 8, *B* and *C*) follows the time course of the temperature jump and is due to a temperature effect on the dye (Martin-Fernandez et al., 1996; 2002). The fluorescence lifetime from Al_{488}-Ad5 stays thereafter approximately constant at a value of ~2.6 ns (Fig. 8 *B*), hence not affected by the change in environmental pH during internalization. This is consistent with the fluorescence of Alexa 488 being independent of pH within the range between pH 4 and pH 10 (Haugland, 2002). In contrast, after the temperature settles at 37°C, the time course of $Al_{488+594}$-Ad5 shows a progressive increase in the fluorescence lifetime, which is not observed for the native or Al_{488}-Ad5 infected cells. Ratioing the time courses displayed in Fig. 8, *B* and *C*, to yield the time course of FRET resulted in the removal of the effect of the temperature change on the donor fluorescence lifetime and revealed the time course of the changes in FRET efficiency at 60 s per datum (Fig. 8 *D*). The time course of FRET shows two kinetic rates, which were fitted by linear regression. The rapid rate shows a half-time ($t_{1/2}$) of ~3 min and arises from the prominent fast increase in donor fluorescence lifetime observed in cells infected with $Al_{488+594}$-Ad5 (*arrow* in Fig. 8 *C*). This early increase in average fluorescence lifetime was consistently detected in the three independent experiments and observed in each of the two fluorescence lifetime components of the biexponential fit (data not shown). The half-time of the slower decrease in FRET efficiency was $t_{1/2} \sim 60$ min.

To investigate whether the observed changes in FRET could be attributed to changes in the relative orientation between donor and acceptors we recorded the time-resolved fluorescence anisotropy decay of Al_{488}-Ad5 in time frames during viral uptake (Lakowicz, 1983). The fluorescence anisotropy of Al_{488}-Ad5 was low (Fig. 9 *A*) most likely signifying free dye rotations (Lakowicz, 1983). This result suggests we can discount unfavorable molecular orientations of the donor with respect to the acceptor that might degrade the accuracy of the FRET measurement. Furthermore, the

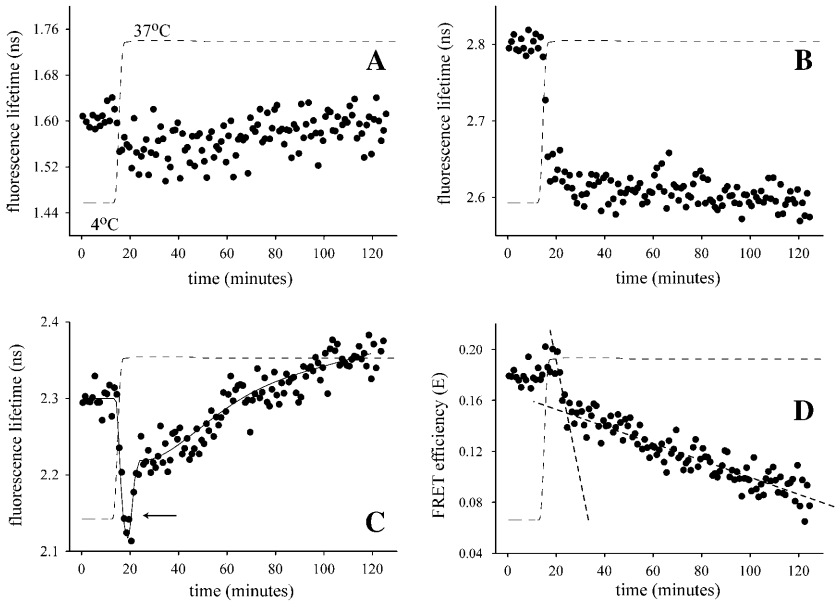

FIGURE 8 (*A*) Time course of the changes with temperature of the fluorescence lifetime of CHO-CAR cells infected with native Ad5 (*solid circles*). Time course of the temperature change (*dashed line*). (*B*) Time course of the fluorescence lifetime from cells infected with Al_{488}-Ad5 analyzed after subtraction of the background. (*C*) Time course of the fluorescence lifetime from cells infected with $Al_{488+594}$-Ad5. The purpose of the continuous line fit is to guide the eye through the time course. (*D*) Time course of FRET efficiency determined from the fluorescence lifetimes of Al_{488}-Ad5 ($\langle\tau_{488}\rangle$) and $Al_{488+594}$-Ad5 ($\langle\tau_{488+594}\rangle$), determined using $E = 1 - (\langle\tau_{488+594}\rangle / \langle\tau_{488}\rangle)$. Results are the mean of three independent experiments with a variance of $<10\%$. Least-squares analysis on the time course of FRET returned two linear regression values ($y = mx + y_o$) of $y_o = 0.32 \pm 0.04$ and $m = -[0.7 \pm 0.2] \times 10^{-2}$ and $y_o = 0.16 \pm 0.02$ and $m = -[0.677 \pm 0.003] \times 10^{-3}$ for the fast and slow rates of FRET decrease, respectively.

anisotropy value remained low in each time frame during Ad5 internalization (data not shown), showing that errors in the donor-acceptor distance, calculated from $R = R_o [E^{-1} - 1]^{1/6}$ (Lakowicz, 1983) where $R_o = 6$ nm is the Förster radius from free dye molecules in solution (Haugland, 2002), are likely to be $<10\%$ (Haas et al., 1978). This calculation returns a mean donor-acceptor distance in $Al_{488+594}$-Ad5 bound to CAR at the cell surface of 7.7 ± 0.7 nm, and shows that the decrease in FRET in Fig. 8 *D* is due to an increase in the distance between donor and acceptors. We therefore conclude that the time course of the efficiency of FRET is accurately reporting on the time course of capsid disassembly.

Additional information on the rotational diffusion of the Alexa 488 molecules was obtained by analyzing the time-resolved anisotropy decay profiles to their components. The best fit was obtained with the biexponential anisotropy decay law plus a static term (Fig. 9 *A*). This analysis shows that Alexa 488 molecules on the Ad5 capsid undertake rotational motions with two correlation times (Fig. 9 *B*). The shorter correlation time reports on rotational motions of Alexa 488 molecules (643 mol wt) around their capsid attachment points. The longer correlation time reports on segmental motions of the fluorophores arising from protein flexibility within the capsid (Lakowicz, 1983). These segmental motions are most likely due to the flexibility of the fibers, a characteristic shown to be crucial for efficient CAR binding (Wu et al., 2003). The static-limiting anisotropy term (r_∞) (Fig. 9, *A* and *C*) results from an energy barrier that limits the extent of rotation of the Alexa 488 molecules. Because of this energy barrier the anisotropy does not decay to zero (Fig. 9 *A*) but to a constant value related to the angle beyond which rotations are not possible (Lakowicz, 1983). The presence of a limiting anisotropy term can be explained by the large virus mass ($\sim 200 \times 10^6$ mol wt; Green, 1970), which prevents significant rotation of the virus during the fluorescence lifetime of the probe, and by the rigidity of the outer icosahedral protein shell of Ad5 (Burnett et al., 1985).

Fig. 9, *B* and *C*, show the time dependence of the anisotropy components during Ad5 entry in CHO-CAR cells. The changes observed in the correlation times were due to the temperature jump (Fig. 9 *B*). In contrast, the value of r_∞ displays a steady reduction as Ad5 internalization progresses, reporting on an increase in the angular range within which the rotations of Alexa 488 molecules on Ad5 are energetically possible. This result can be explained by the progressive dismantling of the capsid reported by FRET (Fig. 8 *D*), which results in an overall increase in protein internal flexibility and allows the dye molecules access to additional rotational motions by which to depolarize the fluorescence emission.

DISCUSSION

The aim of this work has been to develop an assay that allows the determination of the time course of Ad entry and capsid disassembly in real time. We have evaluated this method by measuring the intracellular trafficking of Ad5 and the disassembly of its capsid during uptake in living cells.

The combination of FLIM, FRET, and fluorescence anisotropy data obtained have revealed the detailed time courses of internalization and dissociation of the Ad5 capsid. FLIM data show that Ad5 internalization is inhibited by low temperature (Fig. 4 *A*). In turn, FRET shows that Ad5 capsid disassembly is also inhibited at low temperature in surface-bound virus. This can be concluded from the similarity of the FRET efficiencies from intact Ad5 in solution (Fig. 6 *A*) and that from Ad5 on the cell surface when the cells are maintained at 4°C (Fig. 8 *D*). There was no change in FRET efficiency for ~3 min after the temperature in the cells had

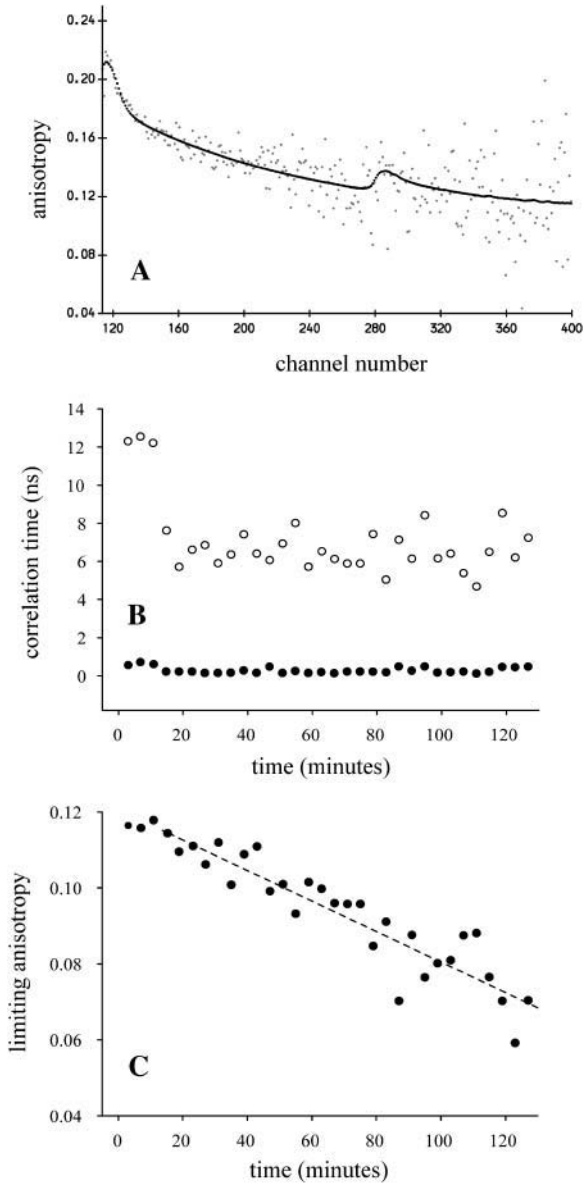

FIGURE 9 (*A*) Example of fluorescence anisotropy decay from Al_{488}-Ad5 bound to CHO-CAR cells at 4°C. The time resolution is 0.079 ns per channel. Anisotropy decays were best fitted with the biexponential anisotropy decay law plus a static term (Lakowicz, 1983): $r(t) = \beta_1 \exp(-t/\phi_1) + \beta_2 \exp(-t/\phi_2) + r_\infty$, where β_i are the relative components of each decay, ϕ_i are the rotational correlation times, and r_∞ the static limiting anisotropy component. The χ^2 values were between 0.9 and 1.16. (*B*) Time course of the correlation times of the fluorescence anisotropy decay data from Al_{488}-Ad5 during cell entry after a temperature jump from 4°C to 37°C, at 4 min per datum. (*C*) Time course of the limiting anisotropy term.

been elevated to the physiological value (Fig. 8 *D*), indicating that the Ad5 capsids also remain intact for this period. This short delay suggests that capsid disassembly proceeds only after some temperature-dependent process, or interaction has occurred. This could in principle be any of a number of events, from clustering of the viruses at the cell surface, to binding to cell surface integrin coreceptors, the signaling cascades that follow, or the membrane ordering required for the onset of endocytosis (Greber, 2002; Greber et al., 1997; Miyazawa et al., 2001; Wickham et al., 1993).

The onset of Ad5 capsid dissociation is accompanied by a biphasic decrease in FRET efficiency, which at the early stages shows a rate of dissociation with a $t_{1/2}$ of ~3 min (Fig. 8 *D*). We have found that 9% of Alexa dye was incorporated into fibers, 6% into pentons, 73% into hexons, with the remaining 12% being incorporated into protein IX. Therefore, the dissociation events that could account for the initial decrease in FRET are the dissociation of fibers, pentons, and hexons, and the removal of protein IX. However, during the uptake of Ad2 in HeLa cells, capsid disassembly has been shown to occur in discrete steps, the first event being the release of fiber that was 80–85% completed within 10 min from the onset of infection (Greber et al., 1993). As Ad2 and Ad5 are members of the same subgroup C, it is reasonable to conclude that the disassembly time course of Ad5 mirrors that previously found for Ad2 (Miyazawa et al., 1999; 2001). Therefore, the similarity between the time of Ad2 fiber release and the time course of the initial FRET decrease for Ad5 suggests that the fast FRET-efficiency rate is reporting on the time course of fiber dissociation. This conclusion is supported by the absence of a fast initial decrease in the time course of the limiting anisotropy term (Fig. 9 *C*). Unlike the rest of the capsid proteins, the internal motions of the fibers are not restricted because they protrude out from the intact icosahedral Ad5 capsid, to which they are attached only at one point by their N-termini (Burnett et al., 1997, Wu et al., 2003). Flexible fibers can therefore be expected to contribute significantly less to the limiting anisotropy term than pentons and hexons, which are held rigid by the multiple interactions by which they form the facets and vertices in the icosahedral structure, and are further anchored by protein IX and other minor capsid proteins (Burnett et al., 1985; 1997).

Our FLIM pH measurements have shown that ~10 min after the temperature in the cells had been elevated to 37°C most of the viruses were resident in intracellular acidic vesicles (Figs. 3 *B* and 5 *B*). This shows that the time course of the release of Ad5 into the cytosol is significantly slower than the initial rate of FRET decrease. Release of the penton base protein from Ad2 capsid represents the second major step in Ad2 disassembly and this event coincides with the escape of Ad2 into the cytosol (Greber et al., 1993). Therefore our FLIM data again support our conclusion that the initial rate of FRET decrease arises from the dissociation of the fibers from the Ad5 capsid, and not from a mixture of the dissociation of fiber and penton. We were surprised to be able to distinguish the dissociation of fibers, as the fluorescence signal from fibers is only 9% of the total fluorescence from the virus. However, the fact that fiber dissociation occurs with a $t_{1/2}$ ~ 3 min, and is therefore well separated from the other dissociation events (Greber et al., 1993), could explain its prominence in the time course of FRET. It is noticeable that the first phase of FRET decrease

coincides closely with the onset of receptor-mediated endocytosis using the same experimental setup (Martin-Fernandez et al., 2000), and with the time course of internalization reported by FLIM measurement of the pH (Fig. 4). This would indicate that fiber shedding, not only occurs at the cell surface as previously shown (Nakano et al., 2000), but also coincides with the onset of endocytosis.

The fast dissociation event in Ad5 is followed by a second capsid disassembly rate with a $t_{1/2}$ of ~60 min. Protein dissociation events that could account for the second FRET rate are the dissociation of pentons, the removal of protein IX, and the dissociation of hexons. This FRET rate is significantly slower than the time course of penton dissociation reported for Ad2 (Greber et al., 1993), which occurs with a $t_{1/2}$ of ~15 min. In contrast, the removal of scaffolding protein IX, a capsid stabilizing component, and the disassembly of hexon, which together account for 84% of the fluorescence signal have been shown to proceed at a much slower pace ($t_{1/2} > 45$ min) (Greber et al., 1993). From the timing of these events we interpret the second rate of FRET decrease to be reporting mostly on the last two stages of capsid disassembly, the removal of protein IX and the dissociation of hexon. This conclusion is supported by the similarity between the second capsid disassembly rate reported by FRET and time course of the limiting anisotropy term (Figs. 8 *D* and 9 *C*), which reports on the dissociation of the proteins forming the rigid, icosahedral Ad5 capsid. The absence of a distinguishable FRET signature from the penton base is likely due to the combination of the lower level of fluorochrome bound to penton (6%), and that dissociation rates of penton and hexon are so similar as to be indistinguishable at the signal/noise level of the measurement.

Our CLSM and FLIM data show that about half of the internalized Ad5 remnants are localized in the cell cytosol proximal to the nuclear envelop within 60 min of the temperature rise (Figs. 3 *C* and 4 *D*). The second rate of FRET decrease is therefore comparable to the time of arrival of Ad5 particles to the nuclear membrane. This supports the finding by others that hexon dissociation only takes place after virus docking at nuclear pore complexes, as previously shown for Ad2 (Greber et al., 1993; 1997).

In summary, our results show that FRET has potential as a new methodology for the quantitative measurement of the infection process in live cell cultures. FRET measurements have the advantage of being noninvasive and fast, and have provided a better time resolution with much less experimental effort than other more traditional experimental strategies. The acquisition of fluorescence anisotropy data, FLIM, and CLSM data has complemented the FRET results by providing information on molecular rotational motions, environmental pH, and intracellular viral location. This combination of microscopy techniques should facilitate rapid, quantitative investigations into the mechanisms of viral entry and disassembly for different serotypes, chimeric, and replication-deficient adenoviruses in many cell types.

We thank Louise Britnell and Mark Swift for their invaluable assistance throughout this work, and Dr. G. E. Blair for kindly providing us with CHO-CAR cells.

We also thank the Biotechnology and Biological Sciences Research Council for funding synchrotron radiation beam time at the SRS at Daresbury Laboratory and for grant 719/C09632. I. Kirby and G. Santis also thank the BBSRC for financial support (grant 29/B15219).

REFERENCES

Bergelson, J. M., J. A. Cunningham, G. Droguett, E. A. Kurt-Jones, A. Krithivas, J. S. Hong, M. S. Horwitz, L. Crowell, and R. W. Finberg. 1997. Isolation of a common receptor for coxackie B viruses and adenoviruses 2 and 5. *Science*. 275:1320–1323.

Blumenthal, R., P. Seth, M. C. Willingham, and I. Pastan. 1986. PH-dependent lysis of liposomes by adenovirus. *Biochemistry*. 25:2231–2237.

Burnett, R. M. 1997. The structure of adenovirus. *In* Structural Biology of Viruses. W. Chiu, R. M. Burnett, and R. L. Garcea, editors. Oxford University Press, Oxford, UK. 209–238.

Burnett, R. M., M. G. Grütter, and J. L. White. 1985. The structure of the adenovirus capsid. I. An envelope model of hexon at 6 Å resolution. *J. Mol. Biol.* 185:105–123.

Chardonnet, Y., and S. Dales. 1970a. Early events in the interaction of adenoviruses with HeLa cells. Penetration of type 5 and intracellular release of the DNA genome. *Virology*. 40:462–477.

Chardonnet, Y., and S. Dales. 1970b. Early events in the interaction of adenoviruses with HeLa cells. II. Comparative observations of the penetration of type 1, 5, 7, and 12. *Virology*. 40:478–485.

Chroboczek, J., R. W. H. Ruigrok, and S. Cusack. 1995. Adenovirus fiber. *In* The Molecular Repertoire of Adenoviruses. W. Doerfler and P. Bohm, editors. Springer, Berlin, Germany. 163–200.

Day, R. N., and D. W. Piston. 1999. Spying on the hidden lives of proteins. *Nat. Biotechnol.* 17:425–426.

Defer, C., M.-T. Belin, M.-L. Cailler-Boudin, and P. Boulanger. 1990. Human adenovirus-host interactions comparative study with members of subgroups B and C. *J. Virol.* 64:3661–3673.

Gao, G. P., Y. P. Yang, and J. M. Wilson. 1996. Biology of adenovirus vectors with E1 and E4 deletions for liver-directed gene therapy. *J. Virol.* 70:8934–8943.

Green, M. 1970. Oncogenic viruses. *Annu. Rev. Biochem.* 39:701–756.

Greber, U. F. 2002. Signalling in viral entry. *Cell. Mol. Life Sci.* 59:608–626.

Greber, U. F., M. Suomalainen, R. P. Stidwill, K. Boucke, M. W. Ebersold, and A. Helenius. 1997. The role of the nuclear pore complex in adenovirus entry. *EMBO J.* 16:5998–6007.

Greber, U. F., M. Willetts, P. Webster, and A. Helenious. 1993. Stepwise dismantling of Ad-2 during entry into cells. *Cell.* 75:477–486.

Haas, E., E. Katchalski-Katzir, and I. Z. Steinberg. 1978. Effect of the orientation of donor and acceptor on the probability of energy transfer involving electronic transitions of mixed polarisation. *Biochemistry*. 17:5064–5070.

Haugland, R. P. 2002. Handbook of Fluorescent Probes and Research Products, 9th ed. Molecular Probes, Eugene, OR.

Hong, S. S., L. Karayan, J. Tournier, D. T. Curiel, and P. A. Boulanger. 1997. Ad-5 fiber knob binds to MHC class 1 α2 domain at the surface of human epithelial and B lymphoblastoid cells. *EMBO J.* 16:2294–2306.

Kirby, I., E. Davison, A. J. Beavil, C. P. Soh, T. J. Wickham, P. W. Roelvink, I. Kovesdi, B. J. Sutton, and G. Santis. 2000. Identification of contact residues and definition of the CAR-binding site of adenovirus type 5 fiber protein. *J. Virol.* 74:2804–2813.

Laemmli, U. K. 1970. Cleavage of structural proteins during the assembly of the head of bacteriophage T4. *Nature*. 227:680–685.

Lakowicz, J. R. 1983. Principles of Fluorescence Spectroscopy. Plenum, New York.

Leopold, P. L., G. Kreitzer, N. Miyazawa, S. Rempel, K. K. Pfister, E. Rodriguez-Boulan, and R. G. Crystal. 2000. Dynein- and microtubule-mediated translocation of adenovirus serotype 5 occurs after endosomal lysis. *Hum. Gene Ther.* 11:151–165.

Leopold, P. L., B. Ferris, I. Grinberg, S. Worgall, N. R. Hackett, and R. G. Crystal. 1998. Fluorescent virions: dynamic tracking of the pathway of adenoviral gene transfer vectors in living cells. *Hum. Gene Ther.* 9: 367–378.

Li, E., D. Stupack, G. M. Bokoch, and G. R. Nemerov. 1998. Adenovirus endocytosis requires actin cytoskeleton reorganisation mediated by Rho family GTPases. *J. Virol.* 72:8806–8812.

Martin-Fernandez, M. L., D. T. Clarke, M. J. Tobin, and G. R. Jones. 2000. Real-time studies of the interactions between epidermal growth factor and its receptor during endocytic trafficking. *Cell. Mol. Biol.* 46:1103–1112.

Martin-Fernandez, M. L., D. T. Clarke, M. J. Tobin, S. V. Jones, and G. R. Jones. 2002. Preformed oligomeric epidermal growth factor receptors undergo an ectodomain change during signalling. *Biophys. J.* 82:2415–2427.

Martin-Fernandez, M. L., M. J. Tobin, D. T. Clarke, C. M. Gregory, and G. R. Jones. 1998. Subnanosecond polarised microfluorimetry in the time domain: an instrument for studying receptor trafficking in live cells. *Rev. Sci. Instrum.* 69:540–543.

Martin-Fernandez, M. L., M. J. Tobin, D. T. Clarke, C. M. Gregory, and G. R. Jones. 1996. A high sensitivity time-resolved microfluorimeter for real-time cell biology. *Rev. Sci. Instrum.* 67:3716–3721.

McDonald, D., L. Stockwin, T. Matzow, M. E. Blair Zajdel, and G. E. Blair. 1999. Coxsackie and adenovirus receptor (CAR)-dependent and major histocompatibility complex (MGH) class I-independent uptake of recombinant adenoviruses into human tumour cells. *Gene Ther.* 6:1512–1519.

Miyazawa, N., P. L. Leopold, N. R. Hackett, B. Ferris, S. Worgall, E. Falck-Pedersen, and R. G. Crystal. 1999. Fiber swap between adenovirus subgroups B and C alters intracellular trafficking of adenovirus gene transfer vectors. *J. Virol.* 7:6056–6065.

Miyazawa, N., R. G. Crystal, and P. L. Leopold. 2001. Adenovirus serotype 7 retention in a late endosomal compartment prior to cytosol escape is modulated by fiber protein. *J. Virol.* 75:1387–1400.

Nakano, M. Y., K. Boucke, M. Suomalainen, R. P. Stidwill, and U. F. Greber. 2000. The first step of adenovirus type 2 disassembly occurs at the cell surface, independently of endocytosis and escape to the cytosol. *J. Virol.* 74:7085–7095.

Nakano, M. Y., and U. F. Greber. 2000. Quantitative microscopy of fluorescent adenovirus entry. *J. Struct. Biol.* 129:57–68.

Wu, E., L. Pache, J. Von Seggern, T.-M. Mullen, Y. Mikyas, P. L. Stewart, and G. R. Nemerow. 2003. Flexibility of the adenovirus fiber is required for efficient receptor interaction. *J. Virol.* 77:7225–7235.

Pastan, I., D. Seth, D. FitzGerald, and M. Willingham. 1986. Adenovirus Entry into Cells: Some New Observations on an Old Problem. Springer-Verlag, New York.

Rauma, T., J. Tuukkanen, J. M. Bergelson, G. Denning, and T. Hautala. 1999. Rab5 GTPase regulates adenovirus endocytosis. *J. Virol.* 73:9664–9668.

Russell, W. C. 2000. Update on adenovirus and its vectors. *J. Gen. Virol.* 81:2573–2604.

Seth, P. 1994. Adenovirus-dependent release of choline from plasma membrane vesicles at an acidic pH is mediated by the penton base protein. *J. Virol.* 68:1204–1206.

Stevenson, S. C., M. Rollence, B. White, L. Weaver, and A. McClelland. 1995. Human adenovirus serotypes 3 and 5 bind to two different cellular receptors via the fiber head domain. *J. Virol.* 69:2850–2857.

Stewart, L. P., C. Y. Chiu, S. Huang, T. Muir, Y. Zhao, B. Chait, P. Mathias, and G. R. Nemerow. 1997. Cryo-EM visualization of an exposed RGD epitope on adenovirus that escapes antibody neutralization. *EMBO J.* 16:1189–1198.

Suomalainen, M., M. Y. Nakano, K. Boucke, S. Keller, R. P. Stidwill, and U. F. Greber. 1999. Microtubule-dependent minus and plus end-directed motilities are competing processes for nuclear targeting of adenovirus. *J. Cell Biol.* 144:657–672.

Trotman, L. C., N. Mosberger, M. Fornerod, R. P. Stidwill, and U. F. Greber. 2001. Import of adenovirus DNA involves the nuclear pore complex receptor CAN/Nup214 and histone H1. *Nat. Cell Biol.* 3:1092–1100.

Van der Oord, C. J. R., G. R. Jones, D. A. Shaw, I. H. Munro, Y. K. Levine, and H. C. Gerritsen. 1996. High-resolution confocal microscopy using synchrotron radiation. *J. Microsc.* 182:217–224.

Van Oostrum, J., and R. M. Burnett. 1985. Molecular composition of the adenovirus type 2 virion. *J. Virol.* 56:439–448.

Wang, K., S. Huang, A. Kapoor-Munshi, and G. Nemerow. 1998. Adenovirus internalisation and infection require dynamin. *J. Virol.* 72: 3455–3458.

Wickham, T. J., E. J. Filardo, D. A. Cheresh, and G. R. Nemerow. 1994. Integrin $\alpha v\beta 5$ selectively promotes adenovirus mediated cell membrane permeabilisation. *J. Cell Biol.* 127:257–264.

Wickham, T. J., P. Mathias, D. A. Cheresh, and G. R. Nemerow. 1993. Integrins $\alpha v\beta 3$ and $\alpha v\beta 5$ promote adenovirus internalization but not virus attachment. *Cell.* 73:309–319.

Yeh, P., and M. Perricaudet. 1997. Advances in adenoviral vectors, from genetic engineering to their biology. *FASEB J.* 11:615–623.